Infection and Immunity

Chronological Aging Is Associated with Biophysical and Chemical Changes in the Capsule of Cryptococcus neoformans

Radames J. B. Cordero, Bruno Pontes, Allan J. Guimarães, Luis R. Martinez, Johanna Rivera, Bettina C. Fries, Leonardo Nimrichter, Marcio L. Rodrigues, Nathan B. Viana and Arturo Casadevall

Infect. Immun. **2011, 79(12):4990. DOI: 10.1128/IAI.05789-11. Published Ahead of Print 3 October 2011.**

INFECTION AND IMMUNITY, Dec. 2011, p. 4990–5000 Vol. 79, No. 12
0019-9567/11/$12.00 doi:10.1128/IAI.05789-11

Chronological Aging Is Associated with Biophysical and Chemical Changes in the Capsule of *Cryptococcus neoformans*▽‡

Radames J. B. Cordero,[1]† Bruno Pontes,[3]† Allan J. Guimarães,[1] Luis R. Martinez,[1,2,6] Johanna Rivera,[2] Bettina C. Fries,[1,2] Leonardo Nimrichter,[5] Marcio L. Rodrigues,[5] Nathan B. Viana,[3,4] and Arturo Casadevall[1,2]*

Department of Microbiology and Immunology[1] and Division of Infectious Diseases of the Department of Medicine,[2] Albert Einstein College of Medicine, Bronx, New York; LPO-COPEA, Instituto de Ciências Biomédicas,[3] Instituto de Física,[4] and Laboratório de Estudos Integrados em Bioquímica Microbiana, Instituto de Microbiologia Professor Paulo de Góes,[5] Universidade Federal do Rio de Janeiro, Rio de Janeiro, Brazil; and Department of Biomedical Sciences, Long Island University-CW, Post, Brookville, New York[6]

Received 10 August 2011/Returned for modification 29 August 2011/Accepted 21 September 2011

Does the age of a microbial cell affect its virulence factors? To our knowledge, this question has not been addressed previously, but the answer is of great relevance for chronic infections where microbial cells persist and age in hosts. *Cryptococcus neoformans* is an encapsulated human-pathogenic fungus notorious for causing chronic infections where cells of variable age persist in tissue. The major virulence factor for *C. neoformans* is a polysaccharide (PS) capsule. To understand how chronological age could impact the cryptococcal capsule properties, we compared the elastic properties, permeabilities, zeta potentials, and glycosidic compositions of capsules from young and old cells and found significant differences in all parameters measured. Changes in capsular properties were paralleled by changes in PS molecular mass and density, as well as modified antigenic density and antiphagocytic properties. Remarkably, chronological aging under stationary-phase growth conditions was associated with the expression of α-1,3-glucans in the capsule, indicating a new structural capsular component. Our results establish that cryptococcal capsules are highly dynamic structures that change dramatically with chronological aging under prolonged stationary-phase growth conditions. Changes associated with cellular aging in chronic infections could contribute to the remarkable capacity of this fungus to persist in tissues by generating phenotypically and antigenically different capsules.

Cryptococcus neoformans is a human fungal pathogen that can cause a fatal chronic meningoencephalitis responsible for more than half a million deaths per year worldwide (38). The virulence of this fungus depends largely on a polysaccharide (PS) capsule that surrounds the entire cell wall and protects the yeast against a wide variety of external insults (46). The importance of the capsule in virulence has made it the target for adjunctive passive immunotherapy and vaccines (28, 39). Our knowledge of the PS capsule is limited by its complexity, the vulnerability of this structure to many analytical methods, and the paucity of techniques available for study of the PS capsule in native states. For example, the capsule is easily damaged by the dehydration required from electron microscopy (10), and the capsular PS is a large heterogeneous polymer that is polydisperse (33) and not amenable to study by X-ray crystallography. Nuclear magnetic resonance (NMR) and biochemical analysis have provided information on the PS composition and local structure (7–9), but many aspects of secondary and tertiary structure remain poorly understood.

C. neoformans is known for its ability to adapt during chronic infection and undergo phenotypical changes (20) that promote persistence and survival inside hosts or specific ecological niches. Examples of such adaptations include melanization (43) and the emergence of giant cells (15, 37, 46), phenomena that enhance the ability of cryptococcal cells to persist *in vivo*. Historically, *in vitro* and *in vivo* studies of the modification in *C. neoformans* capsule have focused mainly on its dimensions (32, 46). Some studies suggested capsule PS modifications based on binding patterns of fluorescent probes (6, 19) and resistance to decapsulation by organic solvents (19) or radiation (31). Brain invasion has been associated with changes in the antigenic structure of the PS capsule that presumably reflect the synthesis of different PS molecules (6). However, no direct evidence for PS structural changes has been reported yet, and the mechanisms involved in these modifications are poorly understood.

In this study, we investigated the effect of chronological aging under prolonged stationary-phase growth conditions on the dynamics of the PS capsule. We note that such aging in nondividing yeast cells (2) is a process fundamentally different from reproductive senescence, which has also been implicated in virulence and persistence for *C. neoformans* (25). Chronological aging refers to the effects of time on a cell after it has stopped growing, whereas generational age refers to the number of daughter cells produced by a given cell. Fungal cellular aging may be important in the pathogenesis of cryptococcosis, since chronicity is associated with the persistence of cells in lung (21) and senescent cells have been shown to accumulate in the course of infection (25). Aging in *C. neoformans* produced capsule changes that were associated with

* Corresponding author. Mailing address: 1300 Morris Park Ave., 411 Forchheimer Bldg., Bronx, NY 10461. Phone: (718) 430-2811. Fax: (718) 430-8968. E-mail: casadeva@aecom.yu.edu.

† Both authors contributed equally to this work.

‡ Supplemental material for this article may be found at http://iai.asm.org/.

▽ Published ahead of print on 3 October 2011.

resistance to phagocytosis by macrophages and antibody (Ab) reactivity.

(The data in this paper are from a thesis to be submitted by R.J.B.C. in partial fulfillment of the requirements for the degree of Doctor of Philosophy in the Sue Golding Graduate Division of Medical Science, Albert Einstein College of Medicine, Yeshiva University, Bronx, NY 10461.)

MATERIALS AND METHODS

Ethics statement. All animal work was done in accordance with animal use protocol approved by the Institutional Animal Care and Use Committee (IACUC) of the Albert Einstein College of Medicine. The Einstein IACUC has approval from the Office of Laboratory Animal Welfare of the National Institutes of Health, assurance number A3312-01. All surgery was performed under xylazine-ketamine anesthesia, and all potential pain and distress were treated/minimized by appropriate use of anesthetic and postoperative analgesics.

Yeast culture. *C. neoformans* serotype A strain H99 (ATCC 208821) was used for all experiments. Cells were grown at 30°C in minimal medium (10 mM $MgSO_4$, 29.3 mM KH_2PO_4, 13 mM glycine, 3 μM thiamine-HCl, pH adjusted to 5.5, and 15 mM dextrose). Chronologically older stationary-phase cells (referred to as old cells) came from a culture grown with agitation for a total of 15 days. At day 13, a new culture was inoculated by taking an aliquot of the culture (1:20 dilution) and regrown in parallel for 2 days until early stationary phase (referred to as young cells). Cell viability was examined in two independent experiments by serial dilution and triplicate plating on Sabouraud dextrose agar plates (Difco Laboratories). After 2 days of incubation at 30°C, the number of colonies was determined.

Elastic-property measurements with optical tweezers. Glass-bottomed dishes were coated with 10 μg ml^{-1} of monoclonal antibody (MAb) 18B7, a mouse IgG1 specific to glucuronoxylomannan (GXM) (5), for 1 h at 37°C. This antibody anchored the yeast cells to the surface of the plate and facilitated experiments with optical tweezers (OT). Suspensions of 10^4 yeast cells in phosphate-buffered saline (PBS) were then added to the plates and incubated for 1 h at room temperature. For some experiments, cell suspensions were incubated with trypsin for 1 h at 37°C, washed with PBS (3 times), and added to the MAb-coated plates. After the plates were washed with PBS to remove nonadherent cells, polystyrene beads (radius, 1.52 ± 0.02 μm) (Polysciences, Warrington, PA) were added to the plate and placed in an OT system equipped with an infrared 1,064-nm Nd:YAG laser (Quantronix, East Setauket, NY) attached to an inverted Nikon Eclipse TE300 microscope (Nikon, Melville, NY). Measurements were performed and Young's modulus values were determined following the procedures previously described (17). Capsule size of probed cells was estimated by measuring the position of the bead (limited by the capsule) relative to the cell wall using ImageJ software (National Institutes of Health, Bethesda, MD).

Capsule size. H99 *C. neoformans* cells were washed (3 times with PBS), mixed with a drop of India ink (BD Biosciences, NJ), and visualized using an Olympus AX 70 microscope (Melville, NY). Capsule size was measured in ImageJ considering the diameter of India ink exclusion zone subtracted by the diameter (×0.5) of the cell wall.

Capsule permeability. *C. neoformans* cells (5×10^6) were washed (3 times with PBS) and placed in tubes containing 100 μl of 200 μg ml^{-1} tetramethylrhodamine (TMR)-labeled dextrans (Molecular Probes, Eugene, OR) of different molecular weights and/or Stokes' radii, as follows: 10,000 (2.8 nm) or 40,000 (4.6 nm) (27). Along with each TMR-dextran, a 2-MDa fluorescein isothiocyanate (FITC)-labeled dextran was added to determine capsule size. The chitin in the cell wall was detected using Uvitex 2B (Polysciences, Warrington, PA) staining. Cells were visualized under fluorescent filters in an Olympus AX 70 microscope (Melville, NY). Fluorescence intensity profiles, cell body diameter (*A*), an apparent whole-cell diameter (*B*) (depicted by the exclusion limits of dextrans by the capsule), and whole-cell diameter (*C*) (see diagram in Fig. 3) were obtained using ImageJ software. A unitless penetration index (PI) was obtained as follows: $(C - A)/(B - A)$.

PS isolation. Capsular PS was isolated by dimethyl sulfoxide (DMSO) extraction (4, 12). Exopolysaccharide (exo-PS) was isolated from the supernatant by filtration (36). PS fractions of different nomial molecular weight limits (NMWl) $10^3 \times 10^3$, >100 kDa, 100 to 10 kDa, and 10 to 1 kDa) were collected by serially concentrating the supernatant through ultrafiltration membranes of different nominal molecular weight limits (NMWL) (100×10^3, 10×10^3, and 1×10^3) using an Amicon (Millipore, Danvers, MA) ultrafiltration cell. The viscous layers of PS formed in membranes were collected, dialyzed, and lyophilized to measure PS amounts that were normalized by volume of filtrate.

Light scattering analysis. The hydrodynamic radius, R_h, of capsular PS preparations was determined by dynamic light scattering (DLS) in a 90Plus/BI-MAS multiangle particle sizing analyzer (Brookhaven Instruments Corp., Holtsville, NY) as described elsewhere (12). The weight-average molecular weight, M_w, and radius of gyration, R_g, were determined by static light scattering (SLS) using a differential refractometer and a molecular weight analyzer (BI-DNDC and BI-MwA, respectively; Brookhaven Instruments, Hotsville, NY) as previously described (12).

Zeta potential. Zeta potential measurements on young stationary-phase and chronologically aged older stationary-phase *C. neoformans* cells (10^6 cells ml^{-1} in 1 mM KCl) were performed in a zeta potential analyzer (ZetaPlus; Brookhaven Instruments Corp., Holtsville, NY) as described elsewhere (22).

Glycosyl composition and NMR spectroscopy. The carbohydrate composition of capsular PS samples was analyzed as described previously (12). For NMR analysis, the sample was partially depolymerized by probe sonication for 30 min at 0°C, subjected to Folch extraction (chloroform-methanol [1:2]) and de-*O*-acetylated (pH 11 NH_4OH) for 20 h at 25°C, and lyophilized. The sample was exchanged in H_2O (99.9% D), lyophilized, and dissolved in 80 μl H_2O (99.96% D). NMR spectra were acquired on a Varian Inova 600-MHz spectrometer at 343 K. The one-dimensional (1D) proton spectrum was processed with linear prediction to 16 K, a 0.65-degree shifted sinebell function, and a Gaussian function (2-Hz line broadening) to obtain a resolution-enhanced, partial spectrum of the region displaying the mannose anomeric protons. Chemical shifts were measured relative to internal 2,2-dimethyl-2-silapentane-5-sulfonic acid (DSS) (d = 0.00 ppm).

Immunofluorescence (IF). The reactivities of two purified and fluorescently conjugated MAbs (AF488-12A1 IgM and AF488-13F1 IgM) with specificity for GXM were determined as previously described (12). These two MAbs originated from one B cell and bind different epitopes (34). Approximately 10^6 young *C. neoformans* cells were biotinylated using EZ Link-Sulfo-NHS-biotin (ThermoScientific, Rockford, IL), intratracheally injected into BALB/c female mice 6 to 8 weeks old (National Cancer Institute), and recovered from lung homogenates 3 days postinfection. Biotin-positive cells were detected with AF594-streptavidin (1 μg ml^{-1}) (Invitrogen). Chitin in the cell wall was visualized using Uvitex 2B. Visualization of α-(1,3)-glucans in the capsule was done using the purified α-(1,3)-glucan antibody MOPC-104E (Sigma, St. Louis, MO) at 15 μg ml^{-1} for 1 h, followed by incubation with 10 μg ml^{-1} of biotin-labeled goat anti-mouse IgM antibody (BD Biosciences) for 30 min. Next, cells were incubated for 30 min in the presence of MAb 18B7-FITC (10 μg ml^{-1}) and AF594-streptavidin (1 μg ml^{-1}) in blocking solution (1% bovine serum albumin [BSA] in PBS). All incubations were done at 37°C. Cells were washed 4 times with PBS between and/or after incubations. Labeled cells were imaged by epifluorescence microscopy on a Zeiss Axioskop 200 inverted microscope using a 63× differential interference contrast (DIC) objective. Collected image processing was done using ImageJ and Voxx (11) software.

Flow cytometry. *C. neoformans* cells (10^6 cells ml^{-1}) labeled with MAbs AF488-12A1 IgM and AF488-13F1 IgM were analyzed with an LSR II BD flow cytometer equipped with lasers emitting at 488, 561, and 635 nm. Data were analyzed with FlowJo software.

ELISA. Enzyme-linked immunosorbent assays (ELISA) were done in 96-well polystyrene plates coated with 50 μl of 1 μg ml^{-1} (in PBS) exo-PS samples (100-, 10-, and 1-kDa fractions) isolated from young and old culture supernatants. After coating, the plates were blocked with 1% BSA in PBS followed by the addition of purified murine anticryptococcus MAbs (18B7-IgG1, 13F1-IgM, 12A1-IgM, and 2D10-IgM). Detection was done with alkaline phosphatase-conjugated goat anti-mouse specific for primary Ab isotypes (Southern Biotechnology) (1 μg ml^{-1} in blocking solution). All incubations were done for 1 h at 37°C. Plates were washed 3 times (TBS-T [10 mM Tris-HCl, 150 mM NaCl, 1 mM NaN_3, 0.1% Tween 20, pH 7.4]) after Ab incubation steps. Reaction mixtures were developed after the addition of *p*-nitrophenyl phosphate disodium hexahydrate, and absorbance at 405 nm was measured in a microplate reader. Binding maxima, B_{max}, and dissociation constants, K_d, were determined by fitting the Ab-PS binding as a function of Ab concentration curves to one-site total binding curves. Goodness of fit for all binding curves was $R > 0.98$.

Phagocytosis. Approximately 2.5×10^4 J774.16 macrophage-like cells/well were plated using complete Dulbecco's modified Eagle's medium (DMEM) in a 96-well microtiter plate and incubated overnight at 37°C in a 10% CO_2 atmosphere under the stimulation of recombinant murine gamma interferon (IFN-γ) and lipopolysaccharide (LPS) at 100 U ml^{-1} and 0.5 μg ml^{-1}, respectively. *C. neoformans* cells were washed (3 times with PBS) and resuspended in DMEM supplemented with 20% mouse serum (Pel-Freez Biologicals, Rogers, AR), incubated for 20 min, added to macrophages (1:5 macrophage-yeast final ratio), and incubated at 37°C for 1.5 h. Complement-mediated phagocytosis was

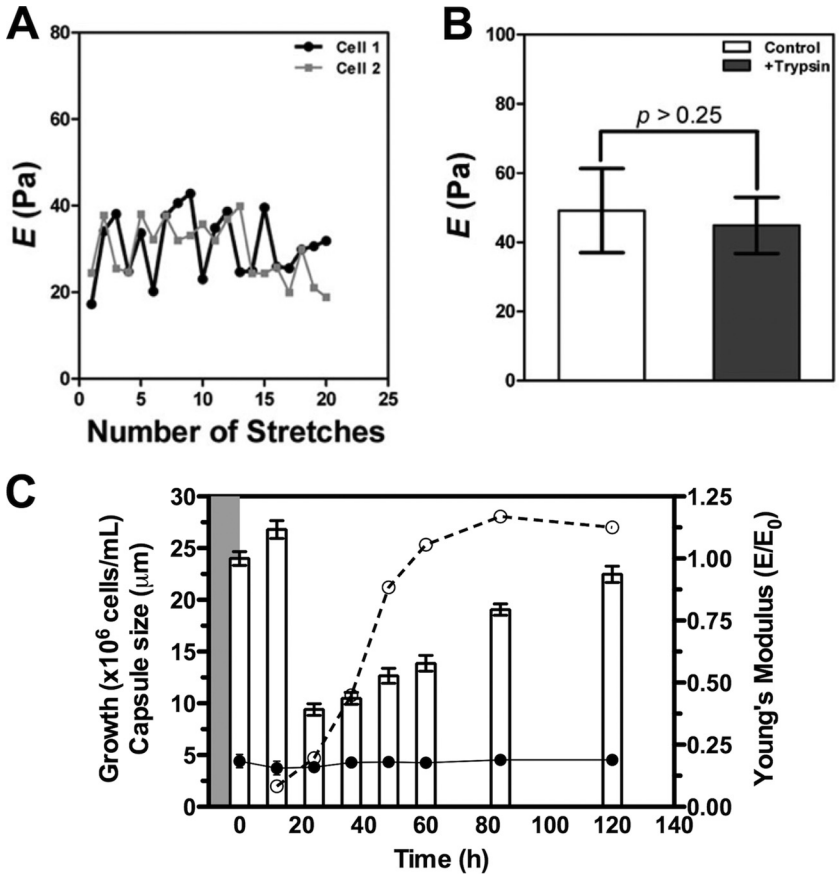

FIG. 1. Analyses of PS capsule elastic properties measured using optical tweezers. (A) Young's modulus variations of two *C. neoformans* yeast cells in 20 repeated stretches. Each point represents one stretch, with its corresponding Young's modulus value. (B) Average Young's modulus of *C. neoformans* cells with or without trypsin protein digestion. Error bars represent standard errors from at least 20 different Young's modulus measured capsules ($P > 0.25$, no significant differences between the two conditions [*t* test]). (C) Average Young's modulus and capsular dimensions as a function of culture age. The white bars represent the relative Young's modulus values during aging in culture, normalized by values at time zero. The values obtained are means ± standard errors from at least 20 different *C. neoformans* PS capsules for each time point. The dashed curve (open circles) represents the growth curve of the *C. neoformans* cells (as number of cells ml^{-1}) during the experiment, as determined by cell counting with a hemocytometer. The continuous curve (closed circles) represents capsule size of probed cells for each time point, estimated by the bead position at the capsule edge. The values obtained are means ± standard errors from at least 20 different *C. neoformans* cells for each time point.

blocked with antibodies against CD18, CD11b, and CD11c (each at 10 μg ml^{-1}) (BD Pharmingen, San Diego, CA). Fixation and staining were done as previously described (12). The percentage of phagocytosis was determined by microscopic analysis and enumeration of macrophages with internalized yeast cells divided by total macrophages. For each condition, at least 300 macrophages were analyzed per well. Experiments were done in quadruplet sets.

Complement deposition. Yeast cells (10^6) were suspended in 100 μl of 20% mouse serum and incubated at 37°C for 1 h. Cells were then washed 3 times with PBS and suspended in blocking solution containing 5 μg ml^{-1} of FITC-conjugated goat anti-mouse C3 antibody (Cappel, ICN, Aurora, OH). Capsule edge and chitin in the cell wall were detected with 18B7-FITC (10 μg ml^{-1}) and Uvitex 2B, respectively. All incubations were done at 37°C for 1 h. Cells were examined under fluorescent filters with an Olympus AX 70 microscope. Fluorescence intensity profiles and relative distances of intensity peaks were analyzed using ImageJ software.

Statistical analysis. Light scattering statistical analyses were performed with 90Plus/BI-MAS software (Brookhaven Instruments Corp., Holtsville, NY). Other statistical analyses (analysis of variance [ANOVA] and Student's *t* test) were performed using GraphPad Prism, version 5.0b (GraphPad Software, San Diego, CA).

RESULTS

Elastic properties of the PS capsule vary with prolonged stationary-phase culture. Our first goal was to determine whether single-cell measurements of capsule elastic properties (*E*), or Young's modulus, using optical tweezers (17), caused irreversible changes to the capsular PSs. Young's modulus measurements from intact *C. neoformans* cell capsules stretched 20 times in a repeated fashion revealed that the values did not significantly change between stretches ($E = 32 \pm 3$ Pa) (Fig. 1A). This result indicated that the PS capsule was elastically deformed, such that one stretch did not affect the subsequent measurements. This finding is consistent with the notion that repeated stretches did not rupture capsular PS molecules. We also found no significant differences in Young's modulus values between control and trypsin-treated *C. neoformans* cells (Fig. 1B). Together, these results demonstrated that the capsular elastic properties are stable and did not change after trypsin treatment.

To evaluate the capsule Young's modulus over time, a *C. neoformans* culture grown in capsule-inducing medium until late stationary phase (day 13) was reinoculated in fresh medium (time zero). Cell samples were collected at different time intervals (up to 120 h postinoculation), and the Young's mod-

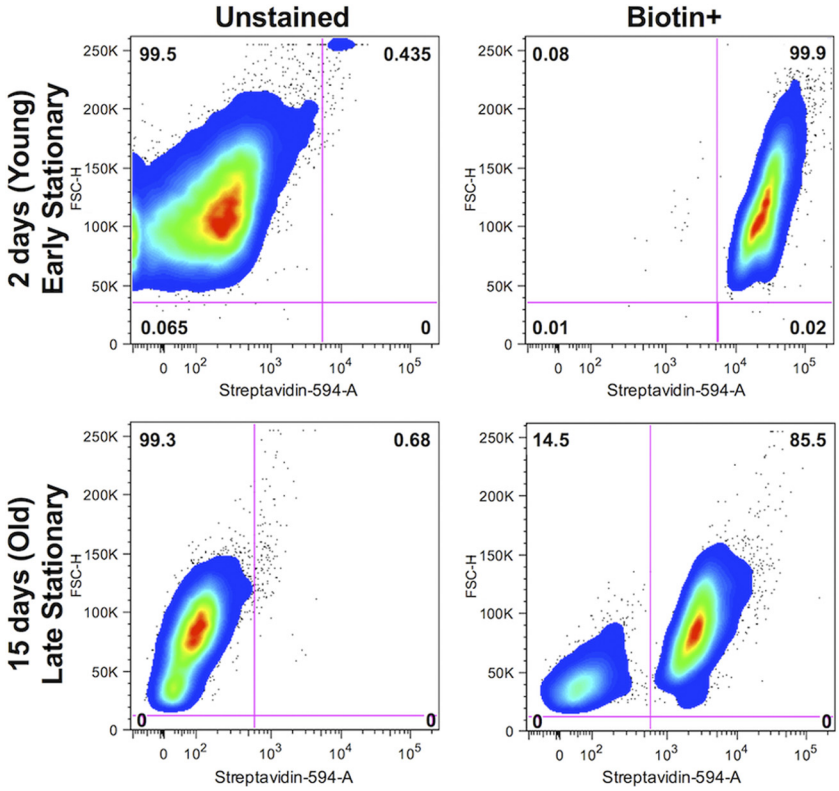

FIG. 2. Fluorescence-activated cell sorter (FACS) analysis of early- and late-stationary-phase cells. Young (early-stationary-phase) cells grown for 2 days were biotinylated and returned to medium. After 15 days of continuous growth, cells were labeled with AF594-conjugated streptavidin and examined. The majority (85.5%) of the initial population of cells (young cells) were still biotin positive after 15 days of growth. Only 14.5% of the cells were streptavidin negative (and thus biotin negative). The *x* axes represent values of streptavidin labeling intensity, and the *y* axes (forward scattering [FSC-H]) represent values of cell diameter.

ulus of the PS capsule was determined. For cells for which we measured the Young's modulus, we also measured capsule size and the population density of the culture from which the cells were obtained. A significant decrease in capsule Young's modulus was detected near 24 h postinoculation (Fig. 1C). A progressive increase was later observed in association with the metabolic phase of the culture and continued even after stationary phase (48 to 120 h), reaching values at 120 h similar to that determined at time zero. However, the size of the capsule showed no significant variation between these time intervals and up to 120 h (Fig. 1C). These results suggest that the Young's modulus of the *C. neoformans* capsule is a modular property, independent of capsule dimension, and that this property changes (increases) over time. This in turn implies major structural changes in capsular PS molecules during cell aging. To further examine this hypothesis and study the biological impact of these capsular changes, we focused on studying early- and late-stationary-phase cells, known to exhibit significant differences in capsule elastic properties.

To maintain consistency and facilitate parallel analysis of both cell states, an early-stationary-phase culture ("young") was inoculated from a late-stationary-phase culture ("old") as described in Materials and Methods. Cells grown until early stationary phase were collected, biotinylated, and returned to the same supernatant. The ratio of biotin-positive and -negative cells was monitored up to 15 days of culture using fluorescence-conjugated streptavidin (Fig. 2). The majority (85.5%) of the cells were still biotin positive after 15 days of incubation and viable (83%) based on CFU evaluation, suggesting that the overwhelming majority of cells in old cultures were still viable and initially present. Slow division during this long stationary-phase incubation period was evident given that a small population of cells (14.5%) was biotin negative. In addition, we noticed a small reduction in mean fluorescence of the cells initially present, which could result from biotin lost during slow division and/or from remodeling or recycling of cell wall structures over time. However, since the overwhelming majority of the cells in the population appeared to be the original biotin-labeled cells, we can consider our early- and late-stationary-phase cultures to represent cell populations of different chronological ages.

Old capsules are less permeable to external solutes. The permeability to fluorescently labeled dextrans of different Stokes' radii and M_w (2.8 nm and 4.6 nm for 10 and 40 kDa, respectively) into capsules exhibiting different elastic properties was determined by measuring the diameter of exclusion zones relative to the capsule size (Fig. 3A to C). Consistent with a higher Young's modulus, capsules from old cells were significantly less permeable to 10- and 40-kDa dextrans than young cells (Fig. 3D). A young culture prepared in parallel, also inoculated from the old culture but grown in fresh medium lacking glucose, was used as a control. The capsule pen-

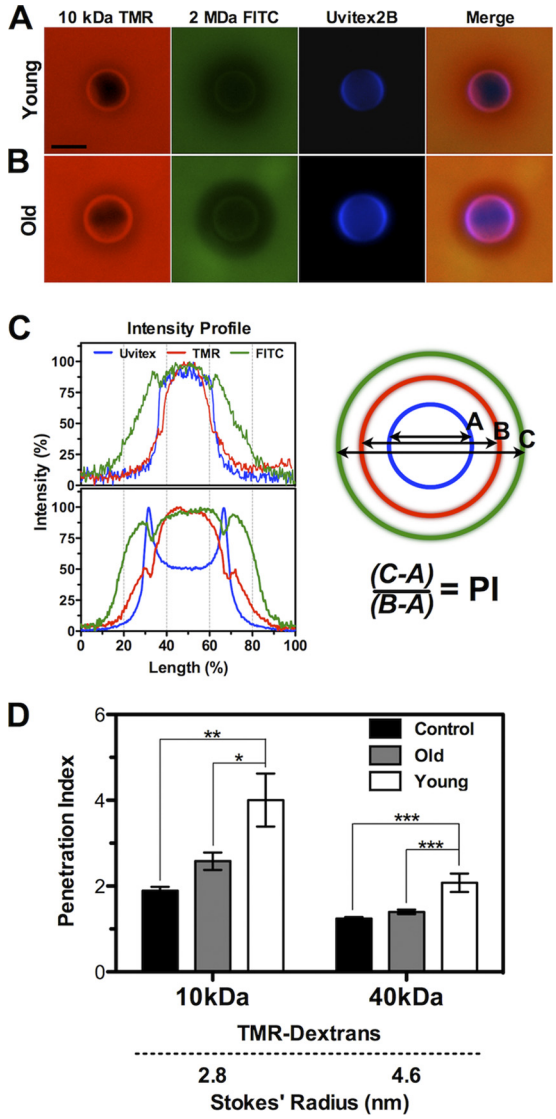

FIG. 3. Capsular permeability as a function of culture age. (A and B) Representative micrographs showing capsule-mediated exclusion of 10-kDa TMR- and 2-MDa FITC-labeled dextrans, cell wall staining by Uvitex 2B, and merge of a young and an old cell. The exclusion zone of this 10-kDa dextran by the capsule is larger for old cells. Bar, 10 μm. (C) Intensity profiles of micrographs shown in panels A (top) and B (bottom). Capsule permeability was analyzed by comparing penetration index (PI) values, obtained by measuring an apparent diameter given by exclusion limits of 10- or 40-kDa TMR-dextrans (length *B*), relative to the cell body diameter (length *A*) and total cell diameter (length *C*) depicted by an exclusion zone obtained with 2-MDa dextrans, which, similarly to India ink particles, are excluded by the capsule. (D) Penetration index of PS capsules from young and old cells, determined using dextrans of different Stokes' radii. Cells reinoculated in minimal medium lacking glucose were used as a control. Capsules of control and old cells were significantly less permeable than those of young cells. Error bars represent standard errors from at least 150 measurements (*, $P < 0.05$; **, $P < 0.01$; ***, $P < 0.001$ [*t* test]).

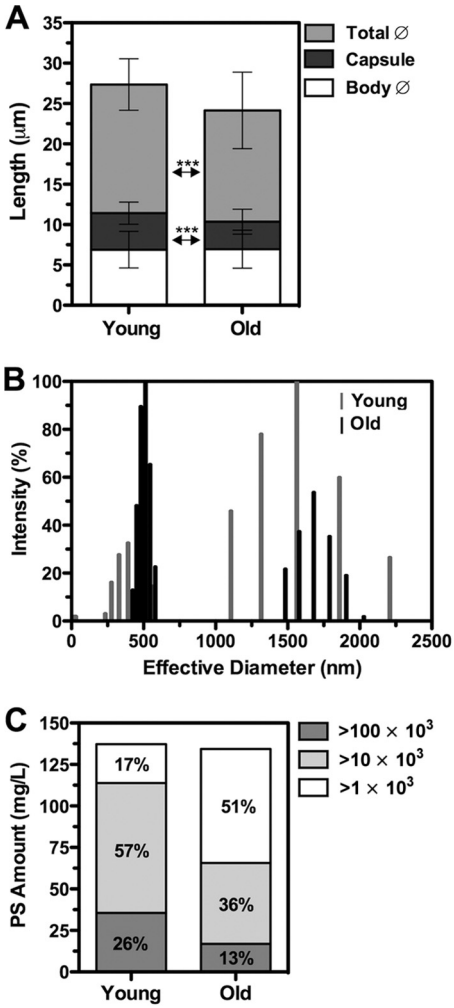

FIG. 4. Dynamics of capsular and supernatant-released PS during prolonged stationary-phase growth. (A) Capsule sizes, bodies, and total cell diameters of chronologically young and old *C. neoformans* H99 cells were determined by light microscopy under India ink staining. Error bars represent standard deviations from 200 measurements (***, $P < 0.001$ [*t* test]). (B) Hydrodynamic size distribution of soluble capsular PS samples DMSO extracted from young and old cells. Data are mean values obtained from duplicates of 10 repeated measurements. (C) Culture supernatants of young and old cells were filtrated using membranes of different NMWL. PS amounts were normalized by volume of filtrate.

etration index of these cells was similar to that of old cells. These results are all in concordance with the elastic properties over time and reemphasize that *C. neoformans* cells manifest important structural modifications on capsular PS molecules that are associated with alterations of capsule permeability. In addition, these results support the dynamic nature of the *C. neoformans* capsule at the structural level and imply an association of this phenomenon with nutrient (dextrose) availability.

Cryptococcal PS structural changes upon prolonged stationary-phase culture. Based on the Young's modulus results and the permeability measurements, we sought to characterize the PS modifications associated with these parameters. Light microscopy of counterstained cell suspensions showed that old cells exhibited smaller capsules and total cellular sizes than young cells (Fig. 4A). No significant differences in cell body diameter were observed. Capsular PS from both cultures (DMSO extraction) was isolated for DLS analysis. The PS

TABLE 1. Age-induced molecular changes in capsular PSs[a]

Sample	*dn/dc* (620 nm)	M_w (g mol^{-1}), $\times 10^6$	R_g (nm)	R_h (nm)	PDI	ρ	Mass density (g mol^{-1} nm^{-1}), $\times 10^4$
Young	0.1502	6.05 ± 0.12	94.6 ± 2.3	417.7 ± 5.4	0.361 ± 0.013	0.23	6.4
Old	0.1523	6.35 ± 0.05	87.9 ± 1.6	325.7 ± 4.7	0.211 ± 0.013	0.26	7.2

[a] Refractive index as a function of concentration (*dn/dc*) in units of ml/g, weight-average molecular weight (M_w), average radius of gyration (R_g), average hydrodynamic radius (R_h), average polydispersity (PDI), shape factor (ρ), and mass density (M_w/R_g) of PS samples. M_w and R_g data are represented as means ± standard deviations (SD) from 3 measurements. R_h and polydispersity data are represented as means ± standard errors (SE) from 10 measurements.

yield recovered from old cells was 29.5% lower than that recovered from younger cells. For both systems, two major hydrodynamic size populations were detected based on scattered intensity: 250 to 580 and 1,125 to 2,250 nm (Fig. 4B). Capsular PS isolated from young cells showed a higher intensity and wider size distribution for the region corresponding to the larger population. A narrow distribution was observed for the region corresponding to the small molecules. The opposite pattern was observed for the capsular PS from old cells (Fig. 4B), which showed lower hydrodynamic size and polydispersity average values (Table 1). These results are consistent with a decrease in capsule size, where capsules from old cells express more PS molecules with lower average hydrodynamic size (Table 1). Furthermore, SLS analysis demonstrated differences in PS molecular conformation. Capsular PS from old cells exhibited higher M_w and lower R_g than that from young cells, which means higher mass density (M_w/R_g) (Table 1). Analysis of the shape factor parameter (ρ) yielded similar values for both samples (Table 1).

Analysis of shed cryptococcal PS (exo-PS) from young and old cultures also showed differences in size. Exo-PS fractions were collected using ultrafiltration membranes of different NMWL (100×10^3, 10×10^3, and 1×10^3). Similar total PS amounts were recovered from supernatants of chronologically young and old cultures (Fig. 4C). Yet, from the young culture supernatant, 26, 57, and 17% of the total PS corresponded to fractions higher than 100×10^3, 100 to 10×10^3, and 10 to 1×10^3, respectively. Surprisingly, the majority (51%) of the exo-PS isolated from the old culture supernatant was in the 10×10^3 to 1×10^3 range (Fig. 4C). These results established a clear difference in the M_w distributions of exo-PS from young and old cultures and demonstrated that, consistent with capsular PS, chronologically old cultures expressed a higher number of PS molecules with smaller dimensions.

Changes in capsule charge and composition with prolonged stationary-phase culture. Zeta potential analysis of *C. neoformans* cells showed significant differences in surface charge between the cultures (Fig. 5A). While surfaces from young cells exhibited an average zeta potential value of −28.08 ± 3.06 mV, old cells showed lower values, with an average of −5.91 ± 1.13 mV (Fig. 5A). Analysis of capsular PS glycosyl composition revealed striking differences. Relative to results for young cells, capsular PS isolated from old cells showed 2.5-, 2.8-, and 3.2-fold mole percent (mol%) decreases in xylose, mannose, and glucuronic acid residues, respectively (Fig. 5B). The differences in glucuronic acid quantities between the cultures were consistent with the decrease in zeta potential values. Interestingly, a significant increase in glucose and galactose residues (5- and 2-fold increases, respectively) and the presence of rhamnose (1.5 mol%), a neutral sugar with immunosuppressor activity (45), were detected in capsular PS isolated from the chronologically old culture.

Immunolabeling of intact cells using purified MOPC-104E IgM, a MAb specific for α-1,3-glucan, showed positive staining for this type of glucan in the capsule (Fig. 5C). A control experiment examining the specificity of MOPC-104E was performed, and in the absence of this antibody, no fluorescence signal was observed (data not shown). A scattered and punctuated labeling pattern, mostly at the capsule periphery, was evident under both conditions (Fig. 5D). The frequency or degree of α-1,3-glucan labeling in the capsule of young and old cells was consistent with the trend observed in glucose amounts detected in capsular PS preparations. The presence of α-glucans was further supported by NMR analysis. A resolution-enhanced 1D proton spectrum showed three major peaks in the anomeric region, at 5.236, 5.305, and 5.164 ppm, revealing that the PS consists mostly of the M2 subunit (see the supplemental material). In addition, an anomeric proton at 5.35 ppm and a corresponding carbon signal at 102.6 ppm were detected, most likely originated from terminal or 4-linked α-glucose. The α-glucose signal was present after extensive dialysis, deacetylation, sonication, and chloroform-methanol extraction, strongly suggesting some association with GXM polymers.

Antibody epitope density and distribution are dynamic and change with aging. The impact of the observed capsular PS structural and physicochemical changes on the reactivity of two MAbs to GXM was analyzed. Capsular immunofluorescence (IF) studies of chronologically young and old cells grown *in vitro* showed different binding profiles depending on the MAb used (Fig. 6A). Relative to the result for young stationary-phase cells, a significant increase in 12A1 binding was observed for old stationary-phase cells. Interestingly, the opposite result was obtained in the case of 13F1 IgM. Different MAb-mediated agglutination results were also observed in concordance with the IF binding intensities. MAbs 13F1 and 12A1 tended to form larger and more aggregates of old and young cells, respectively (Fig. 6B). Differences in epitope binding were also observed after *in vivo* passage. Biotinylated young cells, used for intratracheal infection of mice, were recovered from the lungs after 3 days of infection. Biotin-positive cells (original inoculum) showed higher and lower reactivities for MAbs 12A1 and 13F1, respectively. In contrast, new budded cells (no longer biotinylated) showed lower and higher reactivities for MAbs 12A1 and 13F1, respectively (Fig. 6C). Reactivities of a panel of four anti-GXM MAbs (18B7, 13F1, 12A1, and 2D10) for the exo-PS samples isolated from supernatants and fractionated by ultrafiltration (Fig. 4C) were also examined. Comparative analysis was done by examining the B_{max} and K_d values, derived from MAb binding curves as a function of PS concentration (Fig. 6D). For MAbs 18B7 and 13F1, the K_d

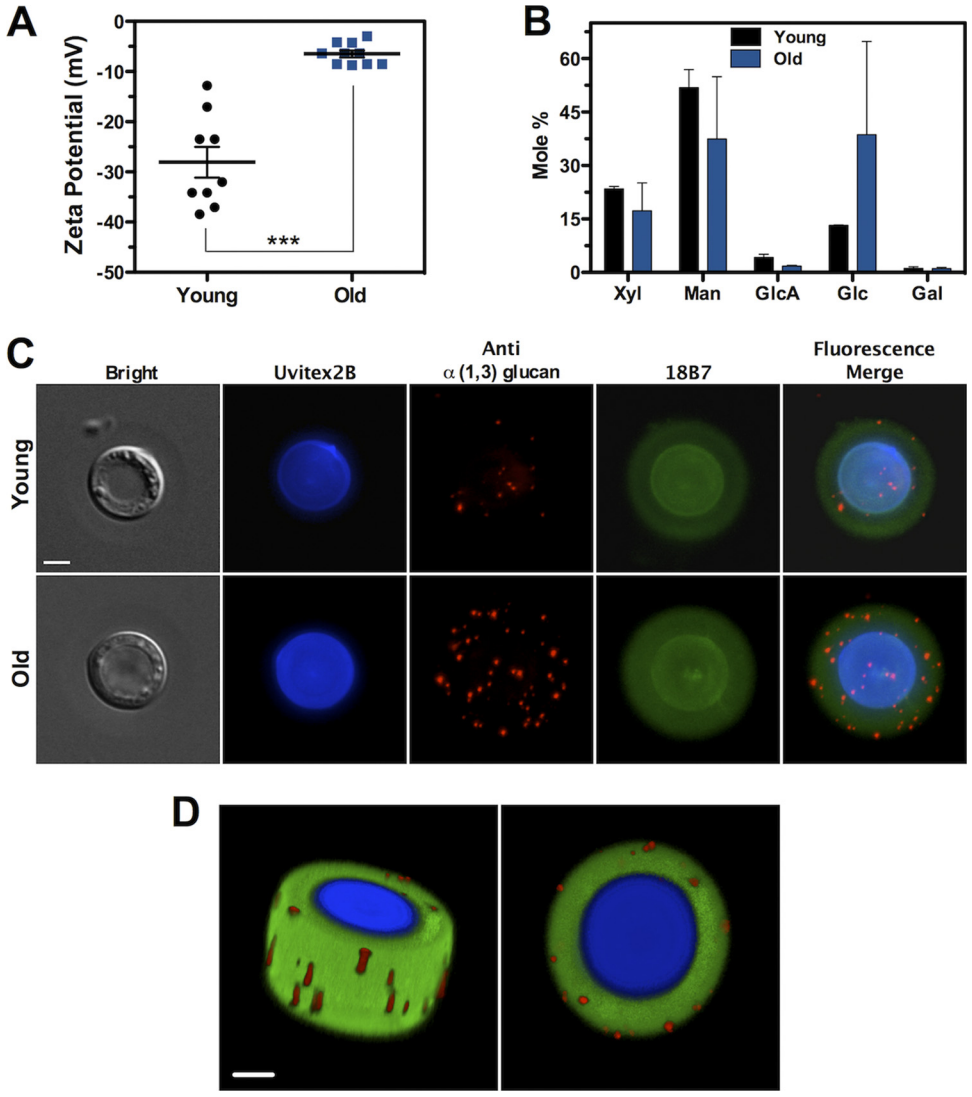

FIG. 5. PS capsule undergoes physicochemical changes during prolonged stationary-phase growth. (A) Zeta potential differences between intact young and old cells. Error bars represent standard errors from 10 repeated measurements (***, $P < 0.001$ [t test]). (B) Glycosyl composition of capsular PS, represented as mol% of xylose (Xyl), mannose (Man), glucuronic acid (GlcA), glucose (Glc), and galactose (Gal) residues. Error bars represent standard errors from two independent experiments. (C) Immunofluorescence micrographs of young and old *C. neoformans* cells labeled with Uvitex 2B (cell wall), purified MAb 18b7 (anti-GXM), and purified MOPC-104E IgM (anti-α-1,3-glucan antibody). Bar, 5 μm. (D) 3D reconstitution of the old cell shown in panel C. Red dots, corresponding to α-1,3-glucans, are predominantly observed close to the capsule outer edge. Bar, 5 μm.

tended to increase with lower PS M_w, for both young and old exo-PS. The opposite was observed for MAbs 12A1 and 2D10. A direct correlation between B_{max} and PS M_w was observed for MAbs 18B7, 12A1, and 2D10, for both young and old exo-PS samples. Interestingly, in the case of 13F1, young stationary-phase and old stationary-phase exo-PSs yielded negative and positive B_{max} and PS M_w correlations, respectively, demonstrating differences in epitope concentration.

Capsular PS structure can impact the ability of macrophages to ingest complement-opsonized *C. neoformans* cells (12). Specifically, cells expressing more linear capsular PS conformations showed higher resistance to phagocytosis (12). Old stationary-phase cells were more resistant to complement-mediated phagocytosis than young cells (Fig. 7A). This difference held true after heat killing of the cells. To confirm that phagocytosis was mediated by complement, we blocked complement receptors, and as expected, phagocytosis was abrogated. Given the differences in phagocytosis and the known differences in capsule elastic properties and permeability, we then examined whether this phenomenon could be explained by differences in C3 deposition on the capsule. Two major differences were evident by epifluorescence microscopy evaluation of C3 capsular deposition when young and old cells were compared. Old stationary-phase cells stained less for complement, and the signal appeared to be localized further away from the cell wall (Fig. 7B), consistent with the decrease in permeability of these capsules.

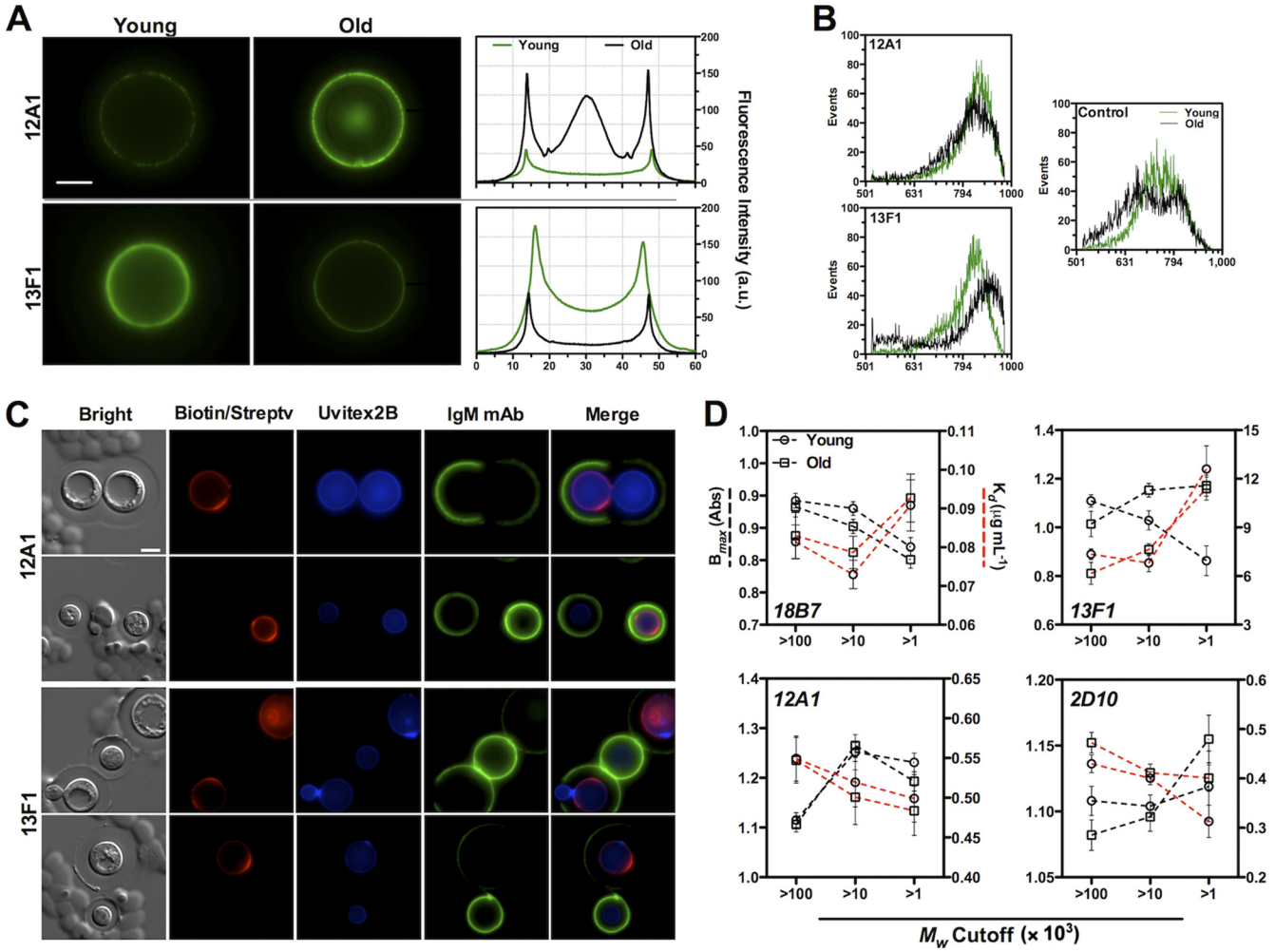

FIG. 6. Dynamics of capsular epitope density upon cell aging. (A) Micrograph representations of young and old cells after labeling with 10 μg ml^{-1} 12A1 IgM and 13F1 IgM anti-GXM MAb. Intensity profiles of fluorescence signal obtained from each antibody are shown on the right. a.u., arbitrary units. Bar, 10 μm. (B) Size and frequency of MAb-mediated aggregates from old and young cells were determined by FACS analysis after capsule labeling with anti-GXM MAbs 13F1 and 12A1. Unlabeled cells were used as a negative control. The graphs represent forward scattering (FSC-H, *x* axis) versus number of cells counted (events, *y* axis). (C) Micrograph representations (2 examples) of AF488-12A1 and AF488-13F1 binding profiles of *C. neoformans* cells recovered from lungs of infected mice 3 days after intratracheal administration. Young cells were biotinylated prior to infection in order to differentiate old and young cells after AF594-streptavidin labeling (red). Bar, 10 μm. (D) Correlation of B_{max} and K_d values of anti-GXM MAbs 18B7-IgG1, 12A1-IgM, 13F1-IgM, and 2D10-IgM with exo-PS samples of different molecular masses recovered from supernatants of young and old cell cultures. Note that M_W cuttoff refers to the NMWL of ultrafiltration membranes. Error bars represent standard errors from triplicates.

DISCUSSION

In this study, we applied a series of biophysical approaches to describe the dynamics of the *C. neoformans* PS capsule as a function of culture age, which for the overwhelming majority of the cells implies increased chronological age. Single-cell analysis using optical tweezers demonstrated that the capsule elastic properties decreased upon prolonged stationary-phase growth, which to some extent mimics chronological aging. These data demonstrate the remarkable capacity of *C. neoformans* to induce structural modifications in capsular PS molecules while maintaining comparable dimensions in capsule size. Comparative analysis of chronologically young stationary-phase and old stationary-phase cells further demonstrated that old stationary-phase cells expressed very different PS capsules characterized by higher Young's modulus values but decreased permeability, PS size and density, and electronegative potential and altered monosaccharide composition. These broad structural changes were associated with altered antibody reactivity to the PS capsule and complement deposition and an increased resistance to complement-mediated phagocytosis by macrophages. Overall, our results demonstrate that the *C. neoformans* PS capsule is highly dynamic and can undergo substantial structural and physicochemical transformations upon prolonged stationary-phase growth, which mimics some of the growth conditions that *C. neoformans* cells encounter during chronic infection on cerebrospinal fluid of patients, which is not a rich growth medium and does not support logarithmic growth (29).

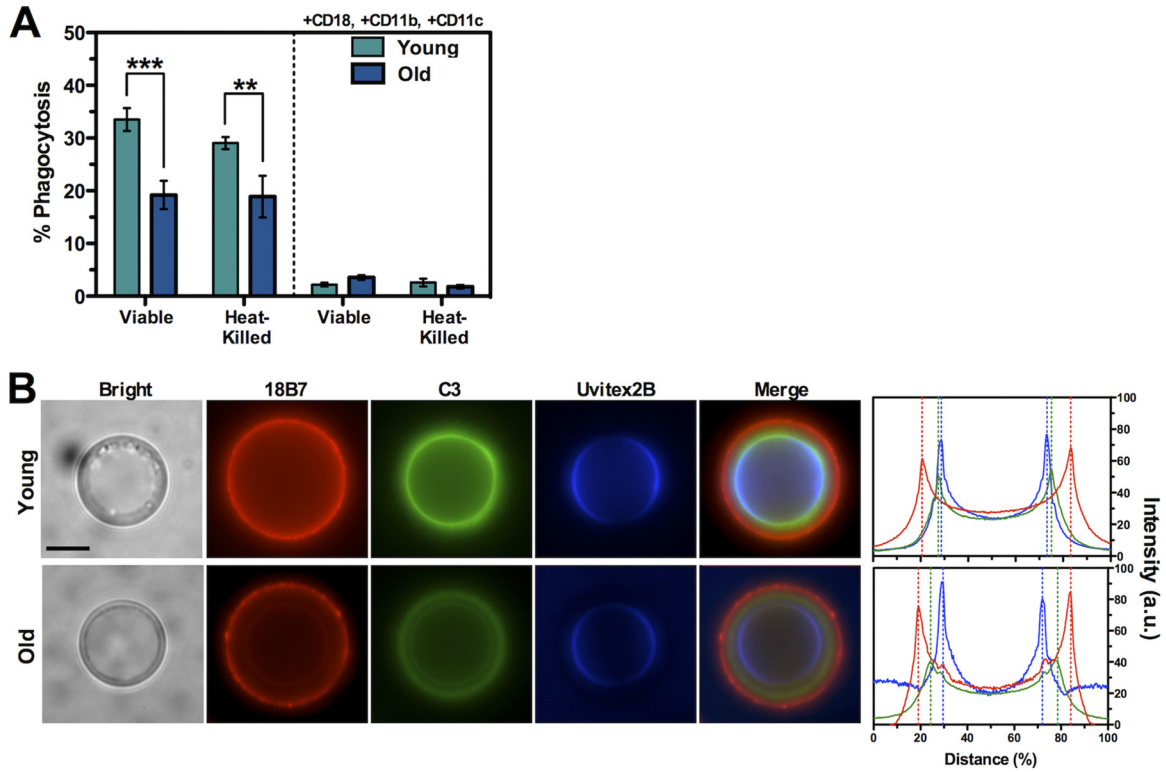

FIG. 7. Resistance to phagocytosis by old *C. neoformans* cells correlates with C3 deposition in the capsule. (A) Old cells are significantly more resistant to complement-mediated phagocytosis by macrophage-like cells even after heat killing treatment. Complement receptor block was used as a control. Error bars represent standard deviations from triplicates (**, $P < 0.01$; ***, $P < 0.001$ [*t* test]). (B) Micrograph representations of young and old cells after opsonization with 20% mouse serum. Capsule edge (red) was detected with MAb 18B7 and TMR-conjugated goat anti-mouse IgG1, and C3 (green) was detected using goat anti-mouse C3 FITC-conjugated antibody. Cell wall (blue) was detected using Uvitex 2B. The images were scanned, and the relative distance of C3 labeling to the cell wall can be observed from the fluorescence signal plot profiles. Bar, 10 μm.

Morphological changes in the capsule of single strains have been of great interest in *C. neoformans* biology and pathogenesis. Indirect evidence suggests that structural modifications of capsular PS can occur at the molecular level in *C. neoformans* cells during infection, as inferred from altered binding patterns of fluorescent probes (6, 19). Moreover, changes in capsular PS structure during aging have been proposed based on increased resistance to decapsulation by organic solvents (19) or gamma radiation (31) of older yeasts. Direct evidence for such structural changes has now been obtained from measurements of capsular elastic properties using optical tweezers, as previously established (17). This approach allows the quantitative study of individual PS capsules in their native state on live *C. neoformans* cells without any drying or fixative procedures that could compromise PS structure. An increase in Young's modulus of capsules exhibiting similar dimensions was observed as cells survived in a prolonged stationary nongrowth or slow growth phase. Consistent with an increase in elastic properties, chronologically older stationary-phase cells exhibit less permeable capsules. The age-related decrease in Young's modulus and permeability of the capsule could be explained by changes in the packing of PS molecules, altering the capsule density and porosity. Mass density derived from SLS analysis of isolated capsular fractions supported this view. Capsular PS from older stationary-phase cells showed higher mass density than PS from younger stationary-phase cells. Interestingly, this increase in mass density did not translate into a higher branching degree of PS molecules, based on their shape factor.

Significant differences in capsule dimensions were also observed between chronologically younger and older stationary-phase cells. The decreased capsule size observed in older stationary-phase cells was not expected based on our initial OT experiments, where capsule sizes remained essentially constant over 120 h postinoculation. Also, previous studies have suggested that, once capsules are formed and/or the maximum size is reached, capsules do not decrease in volume (47). Yet, these studies were done over shorter times and under nutrient-replete conditions, and the decrease in capsule size could be a phenomenon occurring slowly and triggered by depletion of nutrients. The decrease in capsule size observed in older stationary-phase cells was supported by a decrease in average hydrodynamic size of extracted capsular PS and higher quantities of smaller exo-PS molecules recovered from the culture's supernatant. Interestingly, hydrodynamic size for capsular PS and M_w distribution of exo-PS fractions of older stationary-phase cells showed lower polydispersity. Although we do not have an explanation for these observations, it is tempting to speculate the existence of a mechanism involving degradation or remodeling of initial PS structures by local and/or secreted factors, effective and/or triggered during prolonged stationary-

phase culture and nutrient stress. Alternatively, it is possible that extrinsic factors in culture, such as pH, could affect PS structure. We noted, however, that the pH of the culture increased from 5.5 to approximately 6.5 during the course of the chronological aging experiment, excluding the possibility that acidification of the medium could induce modifications in PS structure.

The *C. neoformans* capsule is known to exhibit a strong electronegative potential given by glucuronic acid residues, which appear to be present in relatively high concentrations in the outer region of the capsule (4). Although it has been established that this electronegative potential plays a role in the process of phagocytosis (1, 44), the contribution of charge to virulence in *C. neoformans* is still uncertain. Comparative zeta potential analysis of intact chronologically young and old cells showed significant differences in electronegative potential. Since this parameter is associated with charge, these results suggested chemical modifications in the PS capsule during prolonged stationary-phase growth, highlighting the broad range of capsular dynamics. Indeed, sugar composition analysis of extracted capsular PS revealed major differences in glucuronic acid, mannose, and xylose molar ratios between chronologically younger and older stationary-phase cells. The differences in glucuronic acid content could explain the decrease in capsule electronegativity observed with old cells. Of note, aging was also associated with increased glucose and galactose molar ratios. The increased levels of galactose detected in older stationary-phase cells are consistent with previous studies by our group (13). For the first time, rhamnose residues were detected in PS fractions, exclusively in the capsule of old cells. Rhamnose polymers are of great immunological interest because of their strong immunosuppressive activity (3, 35), and the biological impact on *C. neoformans* remains unknown.

Another major finding in this study was the increased expression of glucose residues in capsular PS fractions of chronologically older stationary-phase cells. NMR analysis in association with immunolabeling studies showed, for the first time, that these correspond to capsular α-1,3-glucans. The presence of glucose in capsular PS preparations was reported previously (16, 22, 42) using various isolation methods, but its presence was thought to reflect contaminating cell wall glucans, anchored to GXM and released during the extraction process (16). Similarly to GXMGal polymers (13, 14, 23), α-1,3-glucans were revealed to be scattered throughout the capsule periphery, although they are localized primarily to the cell wall (26). Alpha glucans are known to be critical to the normal function and integrity of yeast cell walls and play an important role in *C. neoformans* virulence (42) and other fungal pathogens (24, 30, 41). This new *C. neoformans* capsular component could influence initial host-pathogen interactions, as observed in *Histoplasma capsulatum* (40). Although the role of α-1,3-glucans in the capsule is still unknown, the presence and/or exposure of this polymer could present an alternative target for the immune system.

The density of antibody epitopes in the capsule was also observed to change with cell aging. This was clearly illustrated by the differences in reactivity of MAbs 12A1 and 13F1, which are protective and nonprotective, respectively (34), between chronologically young and old capsules. These differences were also observed in *C. neoformans* cells that were passaged *in vivo*. Consequently, chronological aging in *C. neoformans* can affect the expression of protective and nonprotective capsular epitopes. The differences in epitope density were also observed in exo-PS fractions under both conditions. Modifications in epitope accessibility or concentration could be due to changes in PS structure, resulting in steric hindrance, capsular PS shedding, or addition of new structures outside the old one, or could be related to degradation of PS molecules during prolonged culture. Either way, it is dynamic and likely biologically relevant.

The observed capsular changes after prolonged culture were also associated with increased resistance to complement-mediated phagocytosis by macrophages. We demonstrated that this resistance is capsule dependent, since the decrease in phagocytosis of older stationary-phase cells was still observed after heat killing of cells. Furthermore, this effect was shown to result from a decrease in complement deposition on old capsules, which in turn is consistent with the altered capsule permeability observed initially. We want to emphasize that deposition results are pertinent to mouse complement, which was chosen based on the use of a murine macrophage line in the initial phagocytosis experiments. We are aware, however, that C3 deposition in the PS capsule can be influenced by the serum source and that differential localizations between mouse and human sera have been documented (18).

In summary, our results establish that the capsule of *C. neoformans* undergoes major changes in structure, permeability, composition, and antigenic density as a result of prolonged stationary-phase growth. At a practical level, this result indicates that comparative studies of capsular characteristics must carefully control for age of *C. neoformans* cultures. From the viewpoint of pathogenesis, it is noteworthy that cryptococcal infections are usually chronic and long-standing; thus, these observations strongly suggest that prolonged stationary-phase growth and initiation of chronological aging provide yet another mechanism for the generation of structural diversity in cryptococcal populations. Modulation of the PS capsule due to aging and nutrient availability (12) could present a significant advantage to the yeast. Since the PS capsule represents the microbial component first to interact with host cells, capsular dynamics could represent a formidable challenge for hosts to mount an effective response to control the infection.

ACKNOWLEDGMENTS

A.C. and R.J.B.C. were supported by NIH awards AI033774, HL059842, and AI033142. R.J.B.C. was supported in part by the Training Program in Cellular and Molecular Biology and Genetics, T32 GM007491. The Casadevall laboratory participates in the Center for AIDS Research at the Albert Einstein College of Medicine and Montefiore Medical Center funded by the National Institutes of Health (NIH AI-51519). B.P. and N.B.V. were supported by grants from Conselho Nacional de Desenvolvimento Tecnológico (CNPq), Fundação Carlos Chagas Filho de Amparo à Pesquisa do Estado do Rio de Janeiro (FAPERJ), Coordenação de Aperfeiçoamento de Pessoal de Nível Superior (CAPES), and Instituto Nacional de Ciência e Tecnologia de Fluidos Complexos (INCT-FCx). B.P. was supported by a FAPERJ graduate scholarship. M.L.R. and L.N. were supported by grants from the Brazilian agencies CNPq, FAPERJ, FAPESP, CAPES, and FINEP. L.R.M. gratefully acknowledges support of the Long Island University, C.W. Post Campus, Faculty Research Committee. Glycosyl composition and NMR analysis of capsular PS samples were performed at the Complex Carbohydrate Research Center, University of Georgia, supported in part by the Department of Energy (DE-FG-

9-93ER-20097) Center for Plant and Microbial Complex Carbohydrates.

We are thankful to Susana Frases and André Moraes Nicola for technical help with optical tweezers and capsule permeability experiments, respectively.

REFERENCES

1. **Abbracchio, M. P., J. D. Heck, and M. Costa.** 1982. The phagocytosis and transforming activity of crystalline metal sulfide particles are related to their negative surface charge. Carcinogenesis **3:**175–180.
2. **Ashrafi, K., D. Sinclair, J. I. Gordon, and L. Guarente.** 1999. Passage through stationary phase advances replicative aging in Saccharomyces cerevisiae. Proc. Natl. Acad. Sci. U. S. A. **96:**9100–9105.
3. **Baba, T., T. Yoshida, and S. Cohen.** 1979. Suppression of cell-mediated immune reactions by monosaccharides. J. Immunol. **122:**838–841.
4. **Bryan, R. A., et al.** 2005. Radiological studies reveal radial differences in the architecture of the polysaccharide capsule of Cryptococcus neoformans. Eukaryot. Cell **4:**465–475.
5. **Casadevall, A., et al.** 1998. Characterization of a murine monoclonal antibody to Cryptococcus neoformans polysaccharide that is a candidate for human therapeutic studies. Antimicrob. Agents Chemother. **42:**1437–1446.
6. **Charlier, C., et al.** 2005. Capsule structure changes associated with Cryptococcus neoformans crossing of the blood-brain barrier. Am. J. Pathol. **166:** 421–432.
7. **Cherniak, R., R. G. Jones, and E. Reiss.** 1988. Structure determination of Cryptococcus neoformans serotype A-variant glucuronoxylomannan by 13C-n.m.r. spectroscopy. Carbohydr. Res. **172:**113–138.
8. **Cherniak, R., and J. B. Sundstrom.** 1994. Polysaccharide antigens of the capsule of Cryptococcus neoformans. Infect. Immun. **62:**1507–1512.
9. **Cherniak, R., H. Valafar, L. C. Morris, and F. Valafar.** 1998. Cryptococcus neoformans chemotyping by quantitative analysis of 1H nuclear magnetic resonance spectra of glucuronoxylomannans with a computer-simulated artificial neural network. Clin. Diagn. Lab. Immunol. **5:**146–159.
10. **Cleare, W., and A. Casadevall.** 1999. Scanning electron microscopy of encapsulated and non-encapsulated Cryptococcus neoformans and the effect of glucose on capsular polysaccharide release. Med. Mycol. **37:**235–243.
11. **Clendenon, J. L., C. L. Phillips, R. M. Sandoval, S. Fang, and K. W. Dunn.** 2002. Voxx: a PC-based, near real-time volume rendering system for biological microscopy. Am. J. Physiol. Cell Physiol. **282:**C213–C218.
12. **Cordero, R. J., S. Frases, A. J. Guimaraes, J. Rivera, and A. Casadevall.** 2011. Evidence for branching in cryptococcal capsular polysaccharides and consequences on its biological activity. Mol. Microbiol. **79:**1101–1117.
13. **De Jesus, M., S. K. Chow, R. J. Cordero, S. Frases, and A. Casadevall.** 2010. Galactoxylomannans from Cryptococcus neoformans varieties neoformans and grubii are structurally and antigenically variable. Eukaryot. Cell **9:**1018–1028.
14. **De Jesus, M., A. M. Nicola, M. L. Rodrigues, G. Janbon, and A. Casadevall.** 2009. Capsular localization of the Cryptococcus neoformans polysaccharide component galactoxylomannan. Eukaryot. Cell **8:**96–103.
15. **Feldmesser, M., Y. Kress, and A. Casadevall.** 2001. Dynamic changes in the morphology of Cryptococcus neoformans during murine pulmonary infection. Microbiology **147:**2355–2365.
16. **Frases, S., L. Nimrichter, N. B. Viana, A. Nakouzi, and A. Casadevall.** 2008. Cryptococcus neoformans capsular polysaccharide and exopolysaccharide fractions manifest physical, chemical, and antigenic differences. Eukaryot. Cell **7:**319–327.
17. **Frases, S., et al.** 2009. The elastic properties of the Cryptococcus neoformans capsule. Biophys. J. **97:**937–945.
18. **Gates, M. A., and T. R. Kozel.** 2006. Differential localization of complement component 3 within the capsular matrix of Cryptococcus neoformans. Infect. Immun. **74:**3096–3106.
19. **Gates, M. A., P. Thorkildson, and T. R. Kozel.** 2004. Molecular architecture of the Cryptococcus neoformans capsule. Mol. Microbiol. **52:**13–24.
20. **Goldman, D. L., B. C. Fries, S. P. Franzot, L. Montella, and A. Casadevall.** 1998. Phenotypic switching in the human pathogenic fungus Cryptococcus neoformans is associated with changes in virulence and pulmonary inflammatory response in rodents. Proc. Natl. Acad. Sci. U. S. A. **95:**14967–14972.
21. **Goldman, D. L., S. C. Lee, A. J. Mednick, L. Montella, and A. Casadevall.** 2000. Persistent Cryptococcus neoformans pulmonary infection in the rat is associated with intracellular parasitism, decreased inducible nitric oxide synthase expression, and altered antibody responsiveness to cryptococcal polysaccharide. Infect. Immun. **68:**832–838.
22. **Guimaraes, A. J., et al.** 2010. Cryptococcus neoformans responds to mannitol by increasing capsule size in vitro and in vivo. Cell. Microbiol. **12:**740–753.
23. **Heiss, C., J. S. Klutts, Z. Wang, T. L. Doering, and P. Azadi.** 2009. The structure of Cryptococcus neoformans galactoxylomannan contains beta-D-glucuronic acid. Carbohydr. Res. **344:**915–920.
24. **Hogan, L. H., and B. S. Klein.** 1994. Altered expression of surface alpha-1,3-glucan in genetically related strains of Blastomyces dermatitidis that differ in virulence. Infect. Immun. **62:**3543–3546.
25. **Jain, N., et al.** 2009. Isolation and characterization of senescent Cryptococcus neoformans and implications for phenotypic switching and pathogenesis in chronic cryptococcosis. Eukaryot. Cell **8:**858–866.
26. **James, P. G., R. Cherniak, R. G. Jones, C. A. Stortz, and E. Reiss.** 1990. Cell-wall glucans of Cryptococcus neoformans Cap 67. Carbohydr. Res. **198:**23–38.
27. **Lang, I., M. Scholz, and R. Peters.** 1986. Molecular mobility and nucleocytoplasmic flux in hepatoma cells. J. Cell Biol. **102:**1183–1190.
28. **Larsen, R. A., et al.** 2005. Phase I evaluation of the safety and pharmacokinetics of murine-derived anticryptococcal antibody 18B7 in subjects with treated cryptococcal meningitis. Antimicrob. Agents Chemother. **49:**952–958.
29. **Lee, A., et al.** 2010. Survival defects of Cryptococcus neoformans mutants exposed to human cerebrospinal fluid result in attenuated virulence in an experimental model of meningitis. Infect. Immun. **78:**4213–4225.
30. **Maubon, D., et al.** 2006. AGS3, an alpha(1-3)glucan synthase gene family member of Aspergillus fumigatus, modulates mycelium growth in the lung of experimentally infected mice. Fungal Genet. Biol. **43:**366–375.
31. **Maxson, M. E., E. Dadachova, A. Casadevall, and O. Zaragoza.** 2007. Radial mass density, charge, and epitope distribution in the Cryptococcus neoformans capsule. Eukaryot. Cell **6:**95–109.
32. **McFadden, D., O. Zaragoza, and A. Casadevall.** 2006. The capsular dynamics of Cryptococcus neoformans. Trends Microbiol. **14:**497–505.
33. **McFadden, D. C., M. De Jesus, and A. Casadevall.** 2006. The physical properties of the capsular polysaccharides from Cryptococcus neoformans suggest features for capsule construction. J. Biol. Chem. **281:**1868–1875.
34. **Mukherjee, J., G. Nussbaum, M. D. Scharff, and A. Casadevall.** 1995. Protective and nonprotective monoclonal antibodies to Cryptococcus neoformans originating from one B cell. J. Exp. Med. **181:**405–409.
35. **Nair, M. P., and S. A. Schwartz.** 1982. Suppression of human natural and antibody-dependent cytotoxicity by soluble factors from unstimulated normal lymphocytes. J. Immunol. **129:**2511–2518.
36. **Nimrichter, L., et al.** 2007. Self-aggregation of Cryptococcus neoformans capsular glucuronoxylomannan is dependent on divalent cations. Eukaryot. Cell **6:**1400–1410.
37. **Okagaki, L. H., et al.** 2010. Cryptococcal cell morphology affects host cell interactions and pathogenicity. PLoS Pathog. **6:**e1000953.
38. **Park, B. J., et al.** 2009. Estimation of the current global burden of cryptococcal meningitis among persons living with HIV/AIDS. AIDS **23:**525–530.
39. **Pirofski, L. A.** 2001. Polysaccharides, mimotopes and vaccines for fungal and encapsulated pathogens. Trends Microbiol. **9:**445–451.
40. **Rappleye, C. A., L. G. Eissenberg, and W. E. Goldman.** 2007. Histoplasma capsulatum alpha-(1,3)-glucan blocks innate immune recognition by the beta-glucan receptor. Proc. Natl. Acad. Sci. U. S. A. **104:**1366–1370.
41. **Rappleye, C. A., J. T. Engle, and W. E. Goldman.** 2004. RNA interference in Histoplasma capsulatum demonstrates a role for alpha-(1,3)-glucan in virulence. Mol. Microbiol. **53:**153–165.
42. **Reese, A. J., et al.** 2007. Loss of cell wall alpha(1-3) glucan affects Cryptococcus neoformans from ultrastructure to virulence. Mol. Microbiol. **63:** 1385–1398.
43. **Rosas, A. L., et al.** 2000. Synthesis of polymerized melanin by Cryptococcus neoformans in infected rodents. Infect. Immun. **68:**2845–2853.
44. **Tabata, Y., and Y. Ikada.** 1988. Effect of the size and surface charge of polymer microspheres on their phagocytosis by macrophage. Biomaterials **9:**356–362.
45. **Tomsik, P., et al.** 2011. L-rhamnose and L-fucose suppress cancer growth in mice. Cent. Eur. J. Biol. **6:**1–9.
46. **Zaragoza, O., et al.** 2009. The capsule of the fungal pathogen Cryptococcus neoformans. Adv. Appl. Microbiol. **68:**133–216.
47. **Zaragoza, O., A. Telzak, R. A. Bryan, E. Dadachova, and A. Casadevall.** 2006. The polysaccharide capsule of the pathogenic fungus Cryptococcus neoformans enlarges by distal growth and is rearranged during budding. Mol. Microbiol. **59:**67–83.

Editor: G. S. Deepe, Jr.